PHYSICAL REVIEW B **67**, 235307 (2003)

Electronic structure of rectangular quantum dots

E. Räsänen,[1,*] H. Saarikoski,[1] V. N. Stavrou,[1,2] A. Harju,[1] M. J. Puska,[1] and R. M. Nieminen[1]
[1]*Laboratory of Physics, Helsinki University of Technology, P.O. Box 1100, FIN-02015 HUT, Finland*
[2]*Theoretical Quantum Electronics, Institute of Technical Physics, DLR, Pfaffenwaldring 38-40, D-70569 Stuttgart, Germany*

(Received 20 February 2003; published 10 June 2003)

We study the ground-state properties of rectangular quantum dots by using the spin-density-functional theory and quantum Monte Carlo methods. The dot geometry is determined by an infinite hard-wall potential to enable comparison to manufactured, rectangular-shaped quantum dots. We show that the electronic structure is very sensitive to the shape of the dot, and, at realistic sizes, the noninteracting picture determines the general behavior. However, close to the degenerate points where Hund's rule applies, we find spin-density-wave-like solutions bracketing the partially polarized states. In the quasi-one-dimensional limit we find permanent charge-density waves, and at a sufficiently large deformation or low density, there are strongly localized stable states with a broken spin symmetry.

DOI: 10.1103/PhysRevB.67.235307 PACS number(s): 73.21.La, 71.10.−w

I. INTRODUCTION

During the rapid development of nanotechnology, the discoveries in the physics of small electronic structures have concurrently opened new channels in this extremely active field of both theoretical and experimental research. Quantum dots, which fundamentally are confined electron bunches, represent basic components of nanoelectronics. They have been shown to possess many atomlike properties, such as the specific shell structure, determined by the properties of the external confinement.[1]

In lithographically fabricated quantum dots the electrons are strictly confined on the interface of the semiconductor heterostructure, which makes the dot essentially two-dimensional (2D). The lateral confinement, created by adding a voltage to the top gate electrodes, is most commonly approximated by the harmonic oscillator potential. In the isotropic case, this modeling has been shown to lead to a similar addition energy spectrum as measured in the experiments, and adjustments in the model potential have made the agreement even more precise (see Ref. 2 for a review).

Deviations from parabolic confinement have most commonly been studied in connection with the far-infrared response (FIR).[3–7] This is due to the generalized Kohn's theorem,[8,9] stating that FIR couples only to the center-of-mass (c.m.) motion which in the case of a perfect parabolic potential can be separated from the relative motion. Since the c.m. motion has the same energy eigenvalues and dipole resonance frequencies as a single electron, no information on the internal degrees of freedom can be obtained. Ugajin[6] studied FIR absorption for a two-electron square-well quantum dot by using exact diagonalization, and recent density-functional calculations of corner and side modes for triangular and square dots have been done by Valín-Rodríquez *et al.*[7]

The ground-state electronic structure of square-shaped quantum dots was first calculated by Bryant.[10] He used configuration-interaction methods to examine the role of interactions for two electrons. Creffield *et al.*[11] studied polygonal two-electron quantum dots with numerically exact diagonalization, concentrating on the Wigner crystallization,[12] i.e., the localization of the electrons due to the dominant Coulomb interaction in the low-density limit. In our previous work,[13] we found an agreement with their results for polygonal dots by using the spin-density-functional theory (SDFT). We extended the examination to larger electron numbers, including broken spin-symmetry configurations. Those states correspond to spin-density waves (SDW) found in the weak-confinement limit of parabolic quantum dots and represent energetically stable and accurate solutions.[2,14,15] Akbar and Lee[16] also used the SDFT to calculate the addition energy spectrum for square quantum dots with different sizes.

Until now, the study of square-shaped quantum dots with a hard-wall confinement has not been generalized into arbitrary rectangular shapes. However, experiments have been done on rectangular mesas of vertical dots by Austing *et al.*,[17] who applied electron-beam lithography with etching techniques on a double-barrier heterostructure.[18] They measured the addition spectrum with different deformation parameters as well as the magnetic field dependence on the Coulomb oscillations. In the same extensive study, they performed SDFT calculations to simulate the external confinement with an elliptic potential. That approximation was shown to be tentative, though insufficient for a general description of rectangular quantum dots. Lee *et al.*[19] also studied elliptical dots with the SDFT, including additional harmonic confinement in the *z* direction, and obtained similar addition energy spectra.

In the present paper, our secondary aim is to test the ability of a hard-wall external confinement to approximate real rectangular quantum dots, measured in the above-mentioned study. Our main purpose is, however, to clarify the electronic behavior in a rectangular box, beginning from a basic textbook example of quantum mechanics and leading to the discussion of the role of interactions and symmetry-broken solutions in different regimes.

The outline of the paper is as follows. In Sec. II we present the model Hamiltonian and the analytical shell structure of a two-dimensional rectangular box. The computational methods, a real-space SDFT technique and the variational Monte Carlo (VMC) method, are introduced in Sec. III. From the results in Sec. IV, we first give the chemical

potentials and the addition energy spectra of rectangular quantum dots. Then we continue toward a deeper insight into the electronic structure, including the spin behavior in the dot and the quasi-one-dimensional limit. The paper is finished with a summary in Sec. V.

II. MODEL AND THE SHELL STRUCTURE

We define our quantum dot to be two-dimensional, i.e., strictly confined in the z direction. We use the effective-mass approximation (EMA) to describe electrons moving in the plane, surrounded by background material of GaAs with the effective electron mass $m^*=0.067m_e$ and dielectric constant $\epsilon=12.4$. Energies are thus given in Ha$^*\approx 11.8572$ meV and lengths in $a_B^*\approx 9.79$ nm.

The model Hamiltonian of an N-electron system in an external potential can be written as

$$H=\sum_{i=1}^{N}\left[-\frac{\nabla_i^2}{2m^*}+V_{\rm ext}(\mathbf{r}_i)\right]+\sum_{i<j}^{N}\frac{e^2}{\epsilon|\mathbf{r}_i-\mathbf{r}_j|}. \tag{1}$$

The external confinement in the xy plane is described by an infinite hard-wall potential,

$$V_{\rm ext}(x,y)=\begin{cases}0, & 0\leqslant x\leqslant \beta L,\ \ 0\leqslant y\leqslant L\\ \infty, & \text{elsewhere.}\end{cases} \tag{2}$$

Therefore, the area of the dot is βL^2, where the deformation parameter β defines the ratio between the side lengths of the rectangle.

Let us now omit the mutual interactions of the electrons, and consider the single-electron states in a two-dimensional rectangular box. We need two quantum numbers, n_x and n_y, to label all the needed eigenfunctions of two Cartesian coordinates. Inside the box, we can write an explicit formula for these functions as

$$\psi_{n_x,n_y}=\frac{2}{L\sqrt{\beta}}\sin\left(\frac{n_x\pi x}{\beta L}\right)\sin\left(\frac{n_y\pi y}{L}\right). \tag{3}$$

Inserting the eigenfunctions to the stationary Schrödinger equation and setting the area of the rectangle $\beta L^2=\pi^2$ give now the energy eigenvalues in a simple form

$$E_{n_x,n_y}=\frac{1}{2}\left(\frac{n_x^2}{\beta}+\beta n_y^2\right). \tag{4}$$

Figure 1 shows these eigenvalues as a function of β. The degeneracies in the case of $\beta=1$ introduce the magic electron numbers for a square, $N=2,6,8,12,16,20,\ldots$, corresponding to closed shells. When the dot is squeezed, the degeneracies are lifted, resembling the behavior of the single-electron states in an anisotropic harmonic oscillator potential. In the rectangular case, however, one cannot find such regularly located junctions of the eigenstates as in elliptic dots. This is a direct consequence of the more constricted symmetry of rectangular than harmonic quantum dots. This produces remarkable differences in the electron structures as will be shown below. Figure 2 gives the sums of

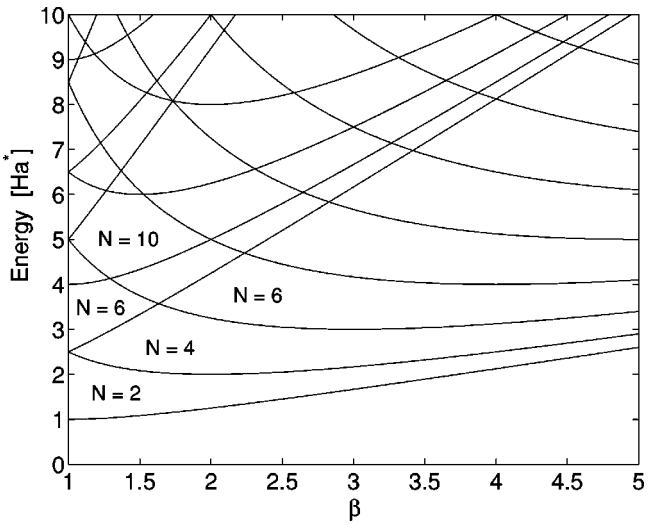

FIG. 1. Lowest single-electron eigenenergies for rectangular quantum dots as a function of the deformation.

the lowest eigenvalues for $N=4,6,\ldots,14$. We can find formation of stable configurations with certain (N,β) combinations as local minima in the total-energy curve. Correspondingly, the cusps indicate degeneracies of the states.

Accumulation of states $(n_x,1)$ at high deformation, which can be seen in Fig. 1, is similar to the formation of Landau bands in the Fock-Darwin energy spectra for the harmonic oscillator potential at high magnetic fields.[20] As the deformation is made stronger, the system becomes gradually quasi-one-dimensional and the occupation of the electrons is determined by the quantization in the longer direction.

III. COMPUTATIONAL METHODS

A. Spin-density-functional theory

We employ the usual self-consistent formulation of the density-functional theory, introduced by Kohn and Sham.[21] The single-electron wave functions are solved within the EMA from

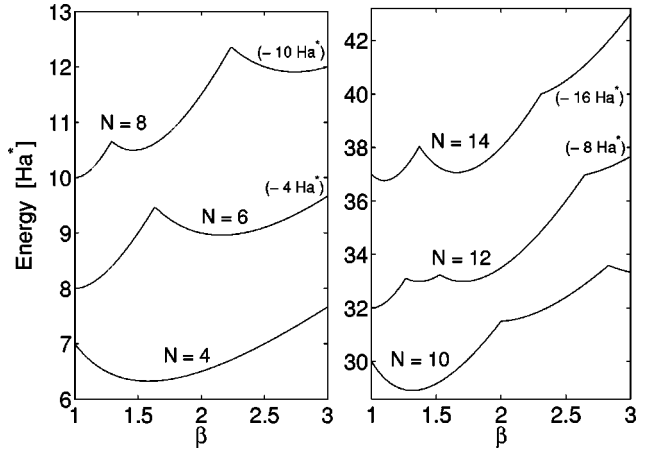

FIG. 2. Sum of the lowest-energy eigenvalues, $\Sigma_{n_x,n_y}\epsilon_{n_x,n_y}$, for $N=4$, 6, 8, 10, 12, and 14 noninteracting electrons as a function of the deformation.

$$\left[-\frac{1}{2m^*}\nabla^2 + V_{\text{eff}}^{\sigma}(\mathbf{r}) \right] \psi_{i,\sigma}(\mathbf{r}) = \epsilon_i \psi_{i,\sigma}(\mathbf{r}), \tag{5}$$

where the effective potential is a sum of the external, Hartree, and exchange-correlation potentials,

$$V_{\text{eff}}^{\sigma}(\mathbf{r}) = V_{\text{ext}}(\mathbf{r}) + V_H(\mathbf{r}) + V_{\text{xc}}^{\sigma}(\mathbf{r}). \tag{6}$$

To calculate $V_{\text{xc}}^{\sigma}(\mathbf{r})$, we use the local spin-density approximation (LSDA),

$$V_{\text{xc}}^{\sigma}(\mathbf{r}) \simeq \frac{\delta E_{\text{xc}}^{\text{LSDA}}}{\delta n_{\sigma}(\mathbf{r})} = \int d\mathbf{r} n(\mathbf{r}) e_{\text{xc}}(n(\mathbf{r}), \zeta(\mathbf{r})), \tag{7}$$

where e_{xc} is the exchange-correlation energy per electron in a uniform electron gas of density $n = n_{\uparrow} + n_{\downarrow}$ and spin polarization $\zeta = (n_{\uparrow} - n_{\downarrow})/n$. We employ a recent analytic parametrization for e_{xc}, formulated in connection with diffusion Monte Carlo calculations (DMC) by Attaccalite *et al.*[22] It is written as

$$e_{\text{xc}}(r_s, \zeta) = e_x(r_s, \zeta) + (e^{-\beta r_s} - 1) e_{\text{x}}^{(6)}(r_s, \zeta) + \alpha_0(r_s) + \alpha_1(r_s)\zeta^2 + \alpha_2(r_s)\zeta^4, \tag{8}$$

where $r_s = 1/\sqrt{\pi n}$ is the density parameter for the 2D electron gas, α's are density-dependent functions of the generalized Perdew-Wang form,[23] $\beta = 1.3386$, and e_x is the exchange energy given as

$$e_{\text{x}}(r_s, \zeta) = -2\sqrt{2}[(1+\zeta)^{3/2} + (1-\zeta)^{3/2}]/3\pi r_s. \tag{9}$$

In Eq. (8), $e_{\text{x}}^{(6)}$ is the Taylor expansion of e_x beyond the fourth order in ζ at $\zeta = 0$.

The above parametrization fits to the DMC simulations over the whole range of spin polarization ($0 \leqslant \zeta \leqslant 1$). This is an essential extension to the often-used parametrization of Tanatar and Ceperley,[24] which is based on DMC calculations for systems with $\zeta = 0$ and 1. Gori-Giorgi *et al.*[25] have shown that the improvement gained with the new parametrization is directly proportional to the electron density and the polarization of the system. In our recent paper,[26] we compare different LSD functionals in small 2D quantum dots. We show that in comparison with the variational quantum Monte Carlo (VMC) calculations, the new parametrization by Attaccalite *et al.* gives more accurate results for the exchange correlation than the forms of Tanatar and Ceperley.

We perform the numerical calculations in real space with two-dimensional point grids without implicit symmetry restrictions. Through this approach, we can shape the external potential almost arbitrarily in the computing region. The number of grid points is 128×128, which gives an error of less than $\sim 1\%$ in the total energy. To accelerate the numerical process, we apply the Rayleigh quotient multigrid method[27] for the discretized single-electron Schrödinger equation (5). A detailed description of this method, generalized to an arbitrary number of lowest eigenenergy states, can be found in Ref. 28.

B. Variational quantum Monte Carlo method

The VMC (Ref. 29) method starts from constructing a trial many-body wave function Ψ with desired properties and with free variational parameters α_i. The parameters are then optimized to converge toward the exact wave function Ψ_0. Using the optimized wave function, the expectation value of an observable A can be evaluated as the average of the corresponding local quantity $\Psi^{-1}A\Psi$. For example, energy is found from the Hamiltonian operator H as

$$E_{\Psi} = \lim_{M \to \infty} \frac{1}{M} \sum_{i=1}^{M} \frac{H\Psi(\mathbf{R}_i)}{\Psi(\mathbf{R}_i)} = \langle \Psi | H | \Psi \rangle, \tag{10}$$

where the N-particle coordinate configurations $\mathbf{R}_i$ are distributed as $|\Psi|^2$ and generated using the Metropolis algorithm.

The variational principle guarantees that the total energy given by the VMC method, using any trial wave function with proper particle symmetry, is always an upper bound for the true total energy of the quantum state in question. The variance of the local energy $\Psi^{-1}H\Psi$ diminishes as the trial wave function approaches an eigenstate of the Hamiltonian, and as a result it can be used not only as a measure of the statistical error in E_{Ψ}, but also as a measure of the difference between the calculated and true energies $E_{\Psi} - E_{\Psi_0}$.

The variational parameters in the trial wave function are optimized by minimizing the total energy. The minimization process itself was done using the stochastic gradient method.[30] The method has proven to be fast and reliable.

The variational wave functions used in this work are of the form

$$\Psi = D_{\uparrow} D_{\downarrow} \prod_{i<j}^{N} J(r_{ij}), \tag{11}$$

where the two first factors are Slater determinants for the two spin types, and J is a Jastrow two-body correlation factor. We neglect the three-body and higher correlations. This has shown to be very accurate in our previous VMC studies (See, e.g., Refs. 31–33). For the Jastrow factor we use

$$J(r) = \exp\left(\frac{Cr}{a + br} \right), \tag{12}$$

where a is fixed by the cusp condition to be 3 for a pair of equal spins and 1 for opposite ones and b is a parameter, different for both spin-pair possibilities. C is the scaled Coulomb strength. The single-particle states in the determinants are taken to be those for the noninteracting problem given in Eq. (3).

IV. RESULTS

A. Addition energy spectra

We calculate the total energies of rectangular dots with different deformation parameters up to 16 electrons. We keep the dot area constant, $A = \pi^2$, through our calculations. The density parameter, defined as $r_s = \sqrt{A/(N\pi)}$ (Ref. 13), thus gets values between 0.44 and 1.8. The electron density in our quantum dots is therefore higher on the average than that of

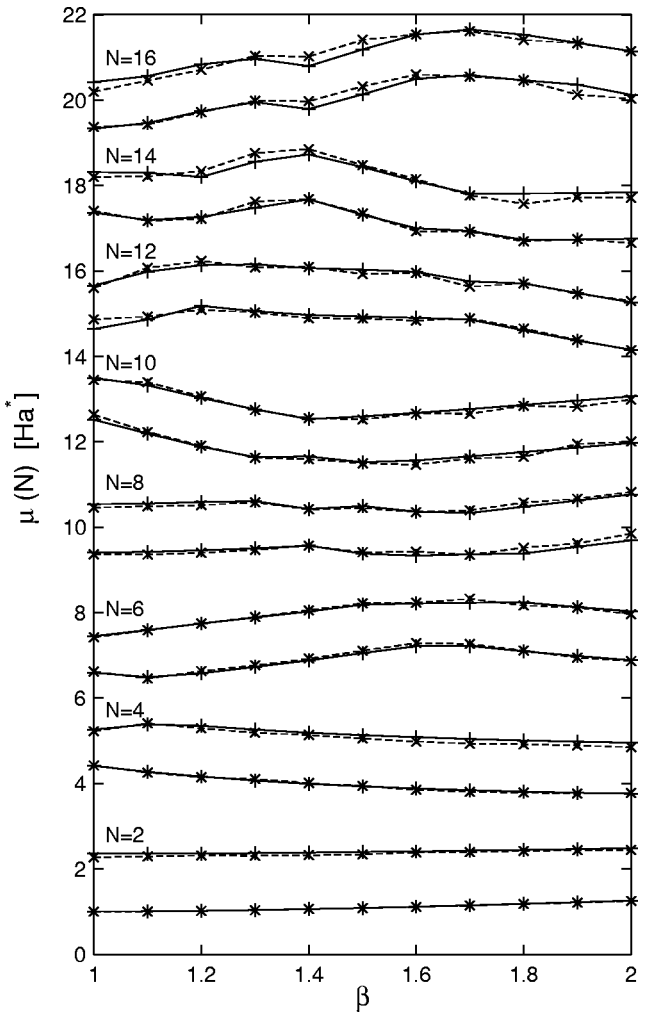

FIG. 3. Calculated chemical potentials for rectangular quantum dots as a function of the deformation parameter. The SDFT and VMC results are given by pluses and crosses connected with solid and dotted lines, respectively.

Austing *et al.*[17] with $r_s=1.5$. Nevertheless, we find that the difference has no noticeable effect on our results. In Fig. 3 we show the SDFT and VMC results for the chemical potentials, $\mu(N)=E(N)-E(N-1)$, $[E(0)$ set to zero$]$, for various values of β. The agreement between the results is good and independent of N and β. As a consequence of the twofold degeneracy in the eigenstates, the pairing of chemical potential values dominates the picture. However, a closer look reveals deviations from this tendency. Due to Hund's rule, near the degenerate points in the single-electron spectrum, the spins of the two highest-energy electrons are parallel and they occupy different states. So, there are regimes in which $\mu(N+1)$ and $\mu(N-1)$ behave in the same way, for example, $N=8$ as $\beta\sim 1.3-1.5$, corresponding to the degeneracy of the states $(n_x,n_y)=(2,2)$ and $(1,3)$. Similar effects in chemical potentials have been observed in measurements of vertical quantum dots in magnetic fields[34] and in calculations of elliptically deformed dots.[19] Due to the rather coarse spacing of our β values in Fig. 3, all the deviations are not observable. A more detailed description as well as a comparison to elliptic dots follow below.

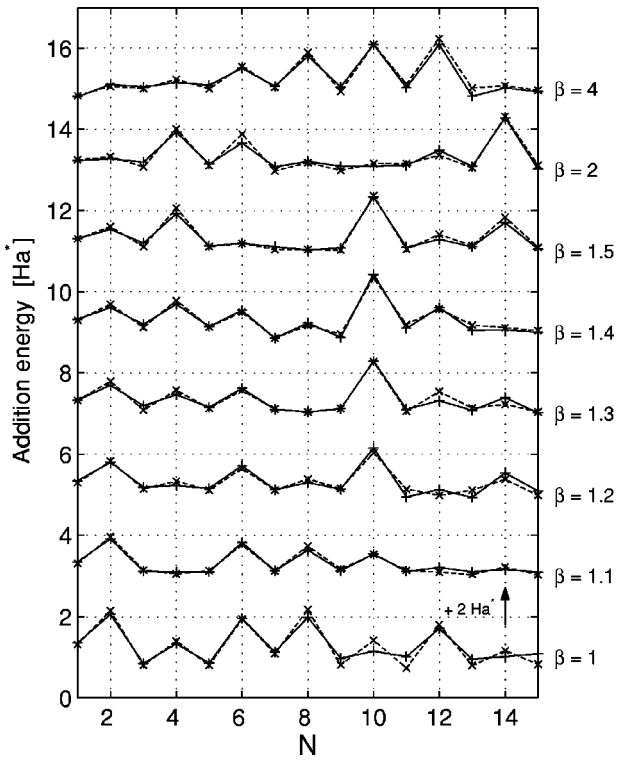

FIG. 4. Addition energy spectra for rectangular quantum dots with different deformation parameters. The SDFT and VMC results are given by pluses and crosses connected with solid and dotted lines, respectively.

In Fig. 4 we show the addition energies $\mu(N+1)-\mu(N)$ for $\beta=1-4$. The spectra obtained with the SDFT and VMC coincide well, especially for $N\lesssim 10$. In the case of a square dot $(\beta=1)$, the magic configurations can be seen as large peaks in the spectrum. For $\beta=1$, the relatively large addition energy for $N=4$ corresponds to a half-filled shell according to Hund's rule. The spectrum agrees well with the results of Akbar and Lee[16] for a square dot of a similar size.

In general, the results for the rectangular quantum dot are very sensitive to the deformation. As β increases, the peaks for $N=4,12$ rapidly vanish but reform above $\beta\simeq 1.2$. For $N=8,14$ the addition energy oscillates more smoothly, and in dots with $N=6,10$ it varies relatively slowly, declining in the former and growing in the latter, in the range $\beta=1-1.5$. Above $\beta\simeq 2$, the formation of an even-odd structure corresponds to the filling of states $(n_x,1)$. In that regime, the growing amplitude in the peaks reflects the increasing spacing between the single-electron eigenstates shown in Fig. 1.

It is intriguing to compare qualitatively the evolution of the spectra in the regime of $\beta\sim 1.3-1.5$ to the experimental results of Austing *et al.*[17] There are two difficulties in the direct comparison. First, the experimental mesa is much larger than the area where the electrons are actually confined, causing uncertainty in the value for the deformation parameter. Second, there are evident irregularities in the experimental dots, leading to unexpected behavior in the spectrum as speculated by Austing *et al.*[17] In spite of these problems, we can generally find similarities in the spectra. Compared with the elliptic case, there is more tendency of forming

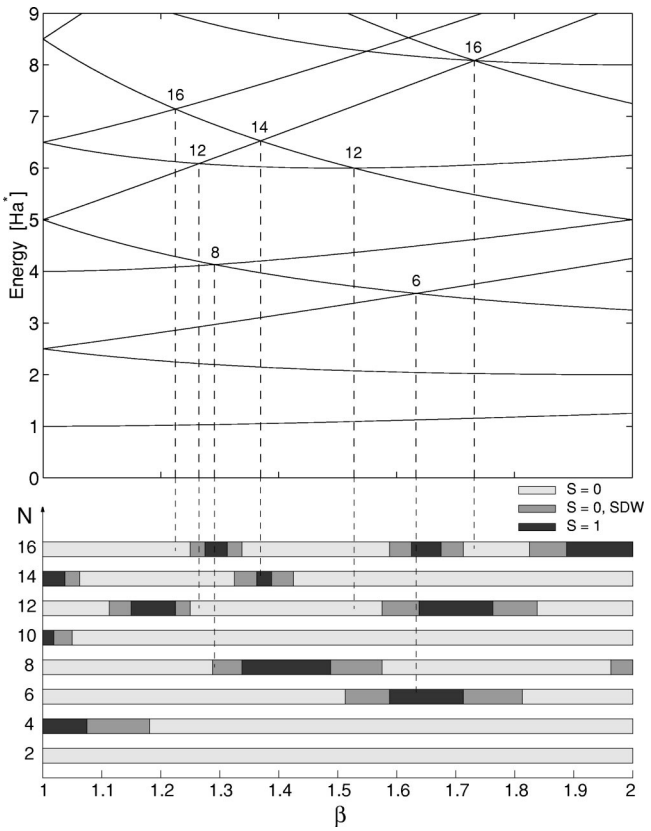

FIG. 5. Noninteracting eigenenergies and the ground-state spins of N interacting electrons for rectangular dots as a function of deformation β.

peaks for even N in both experiments and our approximation at $\beta \sim 1.3$–1.5. This may result from the higher symmetry of the elliptic than rectangular dot, discussed in the context of the single-electron spectrum in Sec. II. Of particular electron numbers, the behavior of the curves for $N=2$,6, and 10 qualitatively agree, and the biggest difference is the rapid disappearance of the peak for $N=4$ at $\beta=1.44$–1.5 in the experiment. Overall, our hard-wall approximation seems to be a slightly better approximation for rectangular-shaped quantum dots than the elliptic description in Ref. 17. However, more accurate comparison than presented here would certainly require more measurements over a wider range for β. An ideal experimental setup would also contain a way to tune β for a single dot, reducing the variation induced by using different dots for different β.

B. Spin development and the role of interactions

Next we consider more carefully the effect of electron-electron interactions on the electronic structure. In Fig. 5 we compare the noninteracting single-electron spectrum with the evolution of the total spin for even N. Due to Hund's rule, we can see partial spin polarization ($S=1$) close to every degenerate point in the single-electron energy spectrum. In the case of a square, the $S=1$ ground state is found correctly for half-filled shells with $N=4$,10, and 14. The spin state changes rapidly to $S=0$ as the dot is squeezed. The range of $S=1$ regimes is obviously directly proportional to the slope

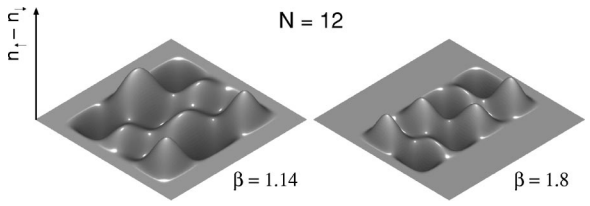

FIG. 6. Spin polarization of a 12-electron rectangular quantum dot in two SDW regimes.

differences of the crossing eigenstates. The triple crossing for $N=16$ at $\beta \approx 1.7$ leads to two separate $S=1$ regimes around the degenerate point. In most cases, polarization occurs at higher β values than the corresponding crossing of the noninteracting states. Therefore, by taking the electron-electron interaction into account, the effective deformation of the rectangle is lower than that of the bare external potential. This is contrary to the result for elliptic dots obtained by Lee *et al.*,[19] who concluded that the interactions tend to strengthen the bare potential by a factor of ~ 1.15–1.25. Intuitively, one would expect just an opposite behavior: in hard-wall rectangular dots the maximum electron density is pushed toward the shorter sides, whereas elliptic and harmonic confinements favor pronounced density at the center. We will present this tendency explicitly in Sec. IV C.

As we show in Fig. 5, every $S=1$ state is bracketed by spin-density-wave-like solutions. In these regimes, the exchange energy gained in the polarized state is relatively close to the cost paid by occupying the higher-energy state. By breaking the internal spin symmetry, the dot gains exchange-correlation energy, which preserves it at the paramagnetic $S=0$ state instead of following Hund's rule with $S=1$. A similar behavior was found in the study of elliptic dots for certain configurations.[17] In the resulting SDW-like solution, the spin-up and spin-down densities are symmetrically coupled with each other as shown in Fig. 6 for a 12-electron dot with $\beta=1.14$ and 1.8, corresponding to two symmetry-broken regimes. In both cases there are six maxima and six minima in the spin polarization, but the shapes of the waves are totally different.

Besides electron densities, it is interesting to consider the development of the Kohn-Sham energy levels near the degenerate point. In Fig. 7 we show the evolution for an eight-electron dot with $\beta=1.2$,1.3,1.4, and 1.5. As can be seen in Fig. 5, these values correspond to states $S=0$, SDW, $S=1$, and SDW, respectively. In the SDW states, the Fermi gap is just large enough to prevent the polarization on the highest occupied level. The phenomenon has an analogy in molecular systems, known as the spontaneous Jahn-Teller effect:[35] any nonlinear molecular system in a degenerate electronic state will be unstable and will undergo distortion to form a system of lower symmetry and lower energy. In this particular case, however, the commonly used argument that the symmetry-broken state would make the electronic structure more stable by the enlargement of the Fermi gap is not precisely valid, as can be concluded from Fig. 7. It is more or less a matter of preserving the $S=0$ state against the transition to the $S=1$ state, representing here a more stable configuration.

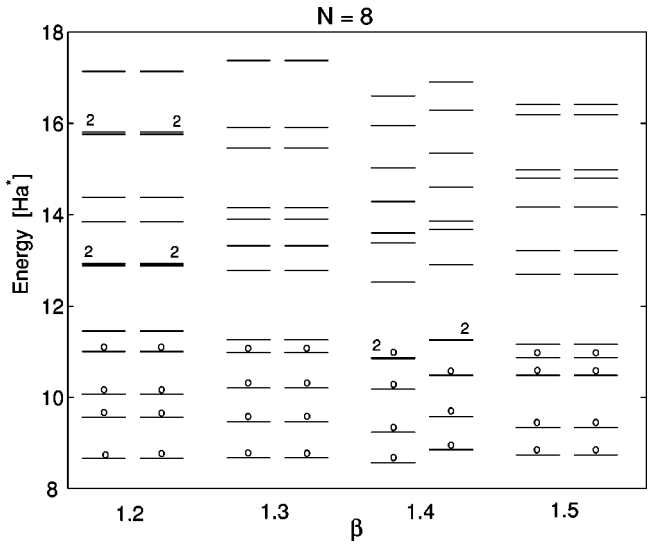

FIG. 7. Development of the Kohn-Sham energy levels for a rectangular eight-electron dot as a function of β. Doubly degenerate levels are denoted by 2 and the occupied states by ○.

The SDW state is a mixture of different $S=0$ states, and there has been a lot of debate if this mixed state is physically meaningful.[2] In our forthcoming studies, which include the exact diagonalization results for $N=4$, we hope to enlighten the validity of the above-represented mixed states for rectangular quantum dots. Until now, however, symmetry-broken solutions have shown their eligibility in several systems. In parabolic quantum dots, for example, the SDW state was found to agree astonishingly well with VMC results in the weak-confinement limit,[15] especially when the latest 2D-LSDA functional was used.[26] In our previous study, we showed that in polygonal quantum dots the breaking of the spin symmetry precedes the complete Wigner molecule formation at low densities.[13] Quantum wires, studied in the context of SDW solutions by Reimann *et al.*,[36] represent another interesting example that we discuss in the following section.

C. Quasi-one-dimensional limit

As the deformation is made larger, electrons in the dot become gradually restricted in the lowest-energy state in the y direction, i.e., only states $(n_x,1)$ are filled. This corresponds to the quasi-one-dimensional limit and a quantum-wire-like electronic structure.[37] Beyond this limit, we find two phases directly observable in the electronic density. First, there is a charge-density wave (CDW) with $N/2$ peaks and preserved spin symmetry. As the deformation or the dot size is increased further, a spin-density wave appears, consisting of interlocked spin-up and spin-down contributions and resulting in a Wigner-molecule-like electron density with N peaks. In Fig. 8 we show examples of both cases with electron-density profiles and the corresponding Kohn-Sham (KS) eigenfunctions. In both wires, the area is still π^2, corresponding to $r_s=0.51$ $(N=12)$ and 0.63 $(N=8)$. As can be seen in the figure, the 12-electron wire with $\beta=10$ retains the spin symmetry and the KS eigenfunctions are doubly degenerate. On the contrary, the eight electron wire with β

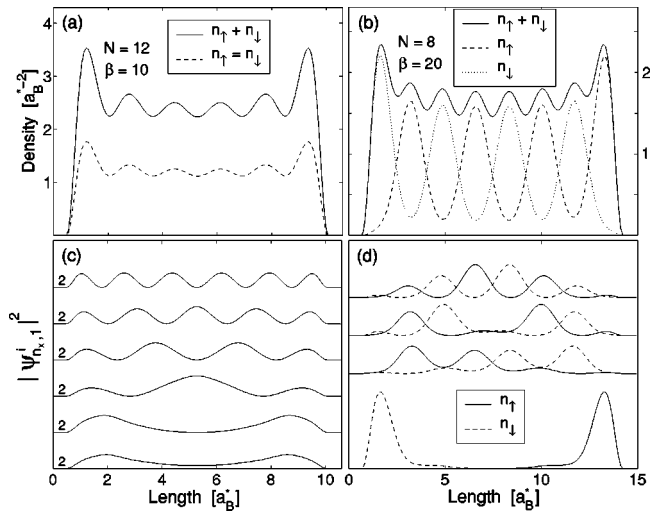

FIG. 8. Electron-density profiles (a,c), and the corresponding single-electron Kohn-Sham eigenfunctions (b,d) for two quantum wires with spin-symmetry preserved and broken ground states. The parameters $(N,\beta,r_s)=(12,10,0.51)$ in (a,b) and (8,20,0.63) in (c,d). Doubly degenerate functions are denoted by the number 2.

$=20$ has a broken spin symmetry. In this case the single-electron KS eigenfunctions are mirror images of each other, and therefore the KS energy levels are still doubly degenerate. Due to the dominating Coulomb interaction, the lowest KS eigenfunctions correspond to localized states near the ends, having 0.16 Ha* lower energy than the other occupied levels with a mutual separation of $\sim$0.06 Ha*. Compared to this, the Fermi gap is particularly large, 0.69 Ha*. In this sense, the breaking of the spin symmetry resembles two-dimensional systems in the low-density limit.[13]

Next we vary both the value of β as well as the density parameter r_s in order to examine the transition point between the two phases discussed above. As shown in Fig. 9 for $N=4$ and 6, the r_s value needed for the deformation to form a SDW decreases as β is increased. The behavior is rather

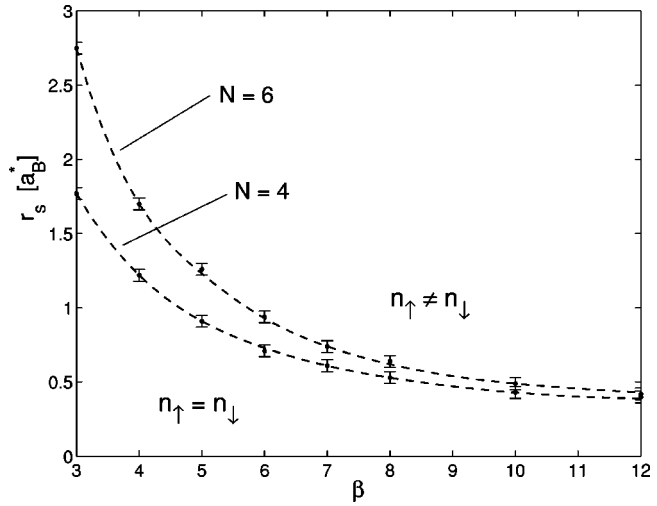

FIG. 9. Phase separation curves between the spin-symmetry-preserved and broken solutions for rectangular quantum dots in the quasi-one-dimensional limit.

insensitive to N; larger electron numbers also qualitatively follow the presented curves with the same tendency of moving slightly up in r_s with increasing electron number, which may arise from our definition for r_s. We point out that beyond the phase separation, i.e., at particularly large β, r_s values, there is also a transition to a fully spin-polarized state not shown in the figure. For example, for a four-electron wire with $\beta = 10$, this occurs at $r_s \sim 1$. In three-dimensional metal nanowires, SDFT calculations have similarly been shown to lead to spontaneous polarization in zero magnetic field at a critical radius of the wire.[38] Recent conductance measurements, performed for ultralow-disorder quantum wires, support this phenomenon.[39] Another remark concerning Fig. 9 is the fact that the ability to reach the quasi-1D limit requires naturally a smaller electron number than the number of the available lowest $(n_x,1)$ states to be occupied. This condition can be easily estimated from the noninteracting single-electron spectrum (Fig. 1).

Comparison between our rectangular hard-wall quantum wires and elliptical wires with harmonic confinement studied by Reimann *et al.*[36] reveals some noticeable differences. First, our LDA (spin-compensated) solution always has a CDW with $N/2$ pronounced maxima, contrary to the elliptic case with a smooth electron density. Second, in rectangular wires the total density distribution is remarkably concentrated at the ends due to the dominating lowest KS eigenstates shown in Fig. 8. The opposite distribution in these two geometries is a direct consequence of the difference in the confining potential: in the elliptic wire, the bowl-like restriction along the wire accumulates a pronounced density at the center, whereas in the hard-wall wire the Coulomb interaction pushes the dominant distribution to the ends. Increasing β or r_s emphasizes this tendency of localization. It is noticeable that the SDW formation is the origin of both the particularly large Fermi gap and the strong localization of the lowest eigenfunctions.

V. SUMMARY

We have investigated the electronic properties of hard-wall rectangular quantum dots. Most calculations have been performed with a symmetry-unrestricted SDFT scheme in real space. For the addition energy spectra, we have done also VMC calculations and found excellent agreement between the two methods. Direct comparison with experiments for rectangular mesas of vertical quantum dots is troublesome, but we find tentative common features in the addition energy spectra. Close to the degenerate points where Hund's rule applies, the states with partial polarization are bracketed by unstable SDW-like solutions. The effective deformation is generally lower than that of a bare potential, but the general picture follows the noninteracting single-electron spectrum. Beyond the quasi-1D limit we find very stable SDW states and extremely strong localization near the ends of the wire, arising from the shape of the hard-wall confinement.

ACKNOWLEDGMENTS

This research was supported by the Academy of Finland through its Centers of Excellence program (2000-2005).

*Electronic address: ehr@fyslab.hut.fi

[1] For an overview, see, e.g., R.C. Ashoori, Nature (London) **379**, 413 (1996); M.A. Kastner, Phys. Today **46** (1), 24 (1993); P.L. McEuen, Science (Washington, DC, U.S.) **278**, 1729 (1997).
[2] S.M. Reimann and M. Manninen, Rev. Mod. Phys. **74**, 1283 (2002).
[3] T. Demel, D. Heitmann, P. Grambow, and K. Ploog, Phys. Rev. Lett. **64**, 788 (1990).
[4] V. Gudmundsson and R.R. Gerhardts, Phys. Rev. B **43**, 12 098 (1991).
[5] D. Pfannkuche and R.R. Gerhardts, Phys. Rev. B **44**, 13 132 (1991).
[6] R. Ugajin, Phys. Rev. B **51**, 10714 (1995).
[7] M. Valín-Rodríquez, A. Puente, and L. Serra, Phys. Rev. B **64**, 205307 (2001).
[8] W. Kohn, Phys. Rev. **123**, 1242 (1961).
[9] P.A. Maksym and T. Chakraborty, Phys. Rev. Lett. **65**, 108 (1995).
[10] G.W. Bryant, Phys. Rev. Lett. **59**, 1140 (1987).
[11] C.E. Creffield, W. Häusler, J.H. Jefferson, and S. Sarkar, Phys. Rev. B **59**, 10 719 (1999).
[12] E.P. Wigner, Phys. Rev. **46**, 1002 (1934).
[13] E. Räsänen, H. Saarikoski, M.J. Puska, and R.M. Nieminen, Phys. Rev. B **67**, 035326 (2003).
[14] M. Koskinen, M. Manninen, and S.M. Reimann, Phys. Rev. Lett. **79**, 1389 (1997).
[15] H. Saarikoski, E. Räsänen, S. Siljamäki, A. Harju, M.J. Puska, and R.M. Nieminen, Eur. Phys. J. B **26**, 241 (2002).
[16] S. Akbar and I.H. Lee, Phys. Rev. B **63**, 165301 (2001).
[17] D.G. Austing, S. Sasaki, S. Tarucha, S.M. Reimann, M. Koskinen, and M. Manninen, Phys. Rev. B **60**, 11 514 (1999).
[18] S. Tarucha, D.G. Austing, T. Honda, R.J. van der Hage, and L.P. Kouwenhoven, Phys. Rev. Lett. **77**, 3613 (1996).
[19] I.H. Lee, Y.H. Kim, and K.H. Ahn, J. Phys.: Condens. Matter **13**, 1987 (2001).
[20] V. Fock, Z. Phys. **47**, 446 (1928); C.G. Darwin, Proc. Cambridge Philos. Soc. **27**, 86 (1930); L. Landau, Z. Phys. **64**, 629 (1930).
[21] W. Kohn and L. Sham, Phys. Rev. **140**, A1133 (1965).
[22] C. Attaccalite, S. Moroni, P. Gori-Giorgi, and G.B. Bachelet, Phys. Rev. Lett. **88**, 256601 (2002).
[23] J.P. Perdew and Y. Wang, Phys. Rev. B **45**, 13 244 (1992).
[24] B. Tanatar and D.M. Ceperley, Phys. Rev. B **39**, 5005 (1989).
[25] P. Gori-Giorgi, C. Attaccalite, S. Moroni, and G.B. Bachelet, Int. J. Quantum Chem. **91**, 126 (2003).
[26] H. Saarikoski, E. Räsänen, S. Siljamäki, A. Harju, M.J. Puska, and R.M. Nieminen, cond-mat/0301062 (unpublished).
[27] J. Mandel and S. McCormick, J. Comput. Phys. **80**, 442 (1989).
[28] M. Heiskanen, T. Torsti, M.J. Puska, and R.M. Nieminen, Phys. Rev. B **63**, 245106 (2001).
[29] W.M.C. Foulkes, L. Mitas, R.J. Needs, and G. Rajagopal, Rev. Mod. Phys. **73**, 33 (2001).
[30] A. Harju, B. Barbiellini, S. Siljamäki, R.M. Nieminen, and G. Ortiz, Phys. Rev. Lett. **79**, 1173 (1997).
[31] A. Harju, V.A. Sverdlov, R.M. Nieminen, and V. Halonen, Phys. Rev. B **59**, 5622 (1999).

[32] A. Harju, S. Siljamäki, and R.M. Nieminen, Phys. Rev. B **65**, 075309 (2002).
[33] S. Siljamäki, A. Harju, V. Sverdlov, P. Hyvönen, and R.M. Nieminen, Phys. Rev. B **65**, 121306 (2002).
[34] S. Tarucha, D.G. Austing, T. Honda, R.J. van der Hage, and L.P. Kouwenhoven, Phys. Rev. Lett. **77**, 3613 (1996).
[35] H.A. Jahn and E. Teller, Proc. R. Soc. London, Ser. A **161**, 220 (1937).
[36] S.M. Reimann, M. Koskinen, and M. Manninen, Phys. Rev. B **59**, 1613 (1999).
[37] E.B. Kolomeisky and J.P. Straley, Rev. Mod. Phys. **68**, 175 (1996).
[38] N. Zabala, M.J. Puska, and R.M. Nieminen, Phys. Rev. Lett. **80**, 3336 (1998).
[39] D.J. Reilly, T.M. Buehler, J.L. O'Brien, A.R. Hamilton, A.S. Dzurak, R.G. Clark, B.E. Kane, L.N. Pfeiffer, and K.W. West, Phys. Rev. Lett. **89**, 246801 (2002).